AeroSense '98, April 13-17, Orlando 1998.
Proc. SPIE, Vol. 3379
Infrared Detectors & Focal Plane Array V. Presentation

Comparison of Intersubband GaAs/AlGaAs Multiple Quantum Well Infrared Photodetectors on GaAs and GaAs-on-Si Substrates

D.K. Sengupta, S.D. Gunapala, T. George, S.V. Bandara, C-N. Chang-Chien, R. Leon, S. Kayali, H.C. Kuo*, W. Fang*, H.C. Liu†, and G.E. Stillman*

Jet Propulsion Laboratory, California Institute of Technology, Pasadena, CA 91109

*Department of Electrical and Computer Engineering,
University of Illinois at Urbana-Champaign, Urbana, IL 61801
†Institute for Microstructural Sciences, National Research Council, Canada K1A OR6

ABSTRACT

We have successfully fabricated intersubband GaAs/AlGaAs quantum well infrared photodetectors grown on GaAs-on-Si substrate and evaluated their structural, electrical, and optical characteristics. We have found that the performance is comparable to a similar detector structure grown on a semi-insulating GaAs substrate. The results are promising for applications in the important 8-12 μm atmospheric window.

Keywords: Quantum well infrared photodetectors, dark current, spectral response, absolute response, GaAs-on-Si substrate.

1. INTRODUCTION

Infrared (IR) photodetection by intersubband absorption using GaAs/AlGaAs quantum wells (QWs) has recently become the subject of extensive investigation [1]. The bound-to-extended state detector concept uses quantum wells with a single bound electron state. Absorption of infrared radiation causes electrons in the bound state to be excited into the extended state, thereby producing a photocurrent. The detector response can be maximized in the range 8-12 μm range by changing the quantum well and the barrier composition. These quantum well detectors have a number of potential advantages with respect to HgCdTe detectors including compatibility with the relatively mature GaAs processing technology, the possibility of monolithic integration with GaAs electronics and the potential to make uniform large area focal plane arrays [2].

GaAs-on-Si technology has promising advantages over GaAs bulk IC's such as higher thermal conductivity, possible expansion of wafer-size, and larger mechanical hardness of substrates. Not only discrete optoelectronic devices but also integrated circuits with satisfactory performance have been successfully fabricated on GaAs-on-Si wafers [3-5]. The growth of quantum well infrared photodetectors (QWIPs) directly on GaAs-on-Si substrates could provide further advantages due to interest in combining Si integrated circuits and GaAs circuits in the same monolithic structure. In such structure, high performance of QWIP can be achieved through the direct integration of Si CMOS signal processing circuits. However, there are some difficulties in epitaxial of GaAs-on-Si: (1) the large lattice mismatch (4%) between GaAs and Si substrate, (2) heteroepitaxial of a polar GaAs layer on nonpolar Si substrates, (3) the differential thermal mismatch between GaAs and Si during cooling from the growth temperature to room temperature. Thus, stresses and high density of dislocation (mismatch dislocation, APD) arise between epitaxial films and the Si substrates. These stresses and dislocations can have important influence on the physical properties of the films and the device performances grown on top of them. Therefore, understanding material and device properties of the GaAs/AlGaAs MQW photodetectors on GaAs-on-Si will be the key issue to develop a reliable technology for QWIP on GaAs-on-Si.

2. EXPERIMENTAL DETAILS

The growth of III-V compound semiconducting epitaxial layers on GaAs-on-Si substrates is now considered to be an important technology. Since there is a relatively large lattice mismatch (4.1%) between GaAs and Silicon, the heterostructure material exhibits a high dislocation density at the hetero interface. The typical defect density is 10^8 ~ 10^9 cm^{-2} near the surface of a 3 μm thick epilayer grown using conventional growth conditions. To reduce the defect density, various methods such as low temperature growth initiation (Akiyama, et. al., 1984), use of tilted Si substrates (Mett, et. al., 1985), and strained layer superlattice buffer layers (Soga, et. al., 1985) have been studied. Most recently, a thermally strained GaAs (TSL) has been used as a buffer layer in MBE growth of GaAs layers on Si substrates (Lee, 1986). To grow

such a buffer layer, the substrate temperature was cycled 4 to 5 times over 200°C within a short period of 3 to 5 minutes. The as-grown GaAs layers were extremely smooth with a defect density of less than $10^5 \sim 10^6$ cm^{-2}. In this work, the TSL technique was used to prepare low defect density GaAs buffer layers on Si substrates. An atmospheric MOCVD system was used to grow GaAs-on-Si substrate. The reactor employs vertical geometry with rf induction heating. The 3 inch Silicon substrates used in this investigation were p-type, oriented two degrees off the (100) axis, with a resistivity of 10-60 Ω cm. The Silicon substrate was first degreased in hot trichloroethane, acetone, and isopropyl alcohol, followed by a deionized (DI) water rinse. Next, the substrates were dipped in a 10:1 DI/HF solution, followed by a rinse in DI water, and then blown dry with warm nitrogen. The wafers were immediately loaded into the reactor and first baked at 900°C in arsine/hydrogen (hydrogen = 10 LPM; arsine = 400 CCM) for 10 minutes (step A). The growth procedure is shown schematically in Fig. 1.

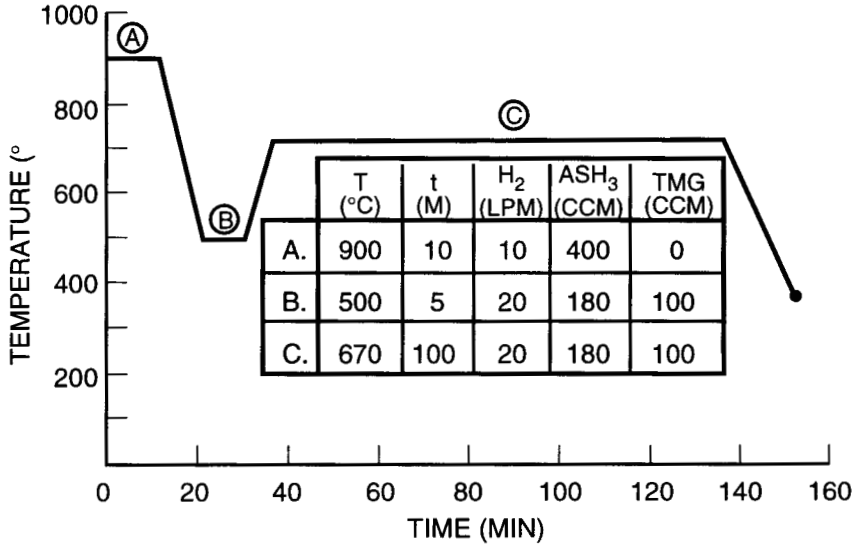

	T (°C)	t (M)	H_2 (LPM)	ASH_3 (CCM)	TMG (CCM)
A.	900	10	10	400	0
B.	500	5	20	180	100
C.	670	100	20	180	100

Fig. 1. *Typical GaAs on Silicon Growth Sequence*

The temperature was then set to 500°C and flow rates were changed for proper growth conditions (step B) (i.e., hydrogen = 20 LPM; arsine = 180 CCM). Trimethyl gallium was introduced (100 S CCM) for a 5 minute growth period with a V/III ratio being 6.9. The temperature was then raised to 670°C for 100 minutes, providing the remainder of the GaAs growth (step C) with a V/III ratio of 1.5. The subsequent growth rate was 5 μm per hour. The resulting GaAs-on-Si material was p-type with carrier concentration in the middle 10^{15} cm^{-3} range. The MQW detectors in the present study were designed to have a strong bound-to-extended electronic transition with a peak absorption located near a wavelength of 9.5 μm. Each detector consisted of 50 40-angstrom wide GaAs quantum wells separated by 300-angstrom wide $Al_{0.25}Ga_{0.75}As$ barriers. The center 20-angstrom region of each well was doped n-type to a concentration of $N_D = 3.3 \times 10^{18}$ cm^{-3} and the outer 10-angstrom of each well was undoped to maintain higher purity at the GaAs/AlGaAs heterojunction. The cladding layer outside of the MQW structure consisted of 1.0 μm thick n^+ layers of GaAs doped $N_D = 1.0 \times 10^{18}$ cm^{-3}. The cladding layer formed either the cathode or anode region of the detector, depending on the polarity of the bias applied to the device. Between the bottom cladding layer and the substrate was a 0.5 μm thick undoped GaAs buffer layer that helped to prevent defects in the Si substrate from propagating up into MQW region. All of the epitaxial layers were grown by solid source molecular beam epitaxy (MBE) at a substrate temperature of 690°C, and the n-type dopant was atomic silicon. To ascertain the effects of using a Si substrate with the MOCVD grown GaAs buffer (QWIP on GaAs-on-Si), the same MQW structure was also grown directly on a semi-insulating GaAs substrate (QWIP on GaAs).

The material quality and optical properties of the QWIP on GaAs and QWIP on GaAs-on-Si samples were investigated using cross-sectional TEM, PL and infrared absorption measurements. TEM was performed with a 120 kV Phillips CM12 microscope. In the PL measurements, the MQW samples were cooled to 77°K and excited with the 632.8 nm line of a HeNe laser. Their luminescence was analyzed by a 0.5 m SPEX monochromator and detected with a liquid nitrogen cooled Ge detector. The intersubband absorption spectrum was measured at room temperature using a DA3 Bomem FTIR spectrophotometer. The MQW samples were polished into multipass waveguides and sandwiched between two infrared-transmitting KRS-5 slabs. IR measurements were done using a glowbar source and a KBr beam splitter. Detection of the infrared beams was achieved using a 77°K photoconductive HgCdTe (MCT) detector.

Quantum well infrared photodetectors were fabricated from QWIP on GaAs and QWIP on GaAs-on-Si samples into 200 μm circular mesas by etching through the upper contact layer and the multiple quantum well structure down to the bottom contact layer. Ohmic contacts to the n-doped contact layers were subsequently formed by evaporating and alloying

AuGe/Ni/Au metallization. All dark current, spectral response and absolute responsivity measurements on these QWIPs were performed with the detectors mounted on a stage which is in thermal contact with the cold end of a continuous flow helium cryostat. The cryostat has an infrared transmitting KRS-5 window which gives the detectors a 2π sr field of view to a 300 K background. In order to set the detectors to the desired operating temperature, a small electrical heating coil was attached to the cold end of the continuous flow helium cryostat, which allows the temperature to be varied from 20 to 350°K with a stability of 0.05°C. The dark current (I-V) characteristics of the QWIPs were measured with a HP4145 semiconductor parameter analyzer at various sample temperatures.

The photocurrent and the optical power were measured in order to calculate the absolute response of the QWIP. The photocurrent, I_p, is obtained for various bias voltages and blackbody apertures. The optical power is determined by integrating the spectral response, S_λ, with the blackbody irradiance, $W(\lambda,T)$. From the two, the absolute response, R_p is calculated as

$$R_p = \frac{I_p}{MF\frac{a^2}{a^2+d^2}A\cos\theta T\int_{6\mu m}^{12\mu m} W(\lambda,T)S_\lambda\, d_\lambda}$$

where A is the QWIP active area, T is the transmission through the KRS-5 window, θ is angle of incident radiation (45°), d is the distance between the blackbody and QWIP, MF is the modulation factor of the blackbody, and a is the aperture radius. The unity gain quantum efficiency, calculated from the absolute response, is given by

$$\eta = \frac{R_p}{\lambda_p}\left(\frac{hc}{q}\right)$$

where R_p is the peak absolute response and λ_p is the peak wavelength in the normalized spectral response.

3. THEORETICAL MODELING

The potential profile for a single period of an as-grown multiple-quantum-well structure is considered to be close to the ideal finite square well. One period of the potential profile V(z) of the actual as-grown AlGaAs/GaAs QWIP and the energies of the lowest three subbands are shown to the scale in Fig. 2(a). From Fermi's Golden Rule, we can derive the intersubband absorption coefficient spectrum of the MQWs structure using the momentum matrix element

$$\alpha(\omega) = \frac{e^2\pi}{n_r c\varepsilon_o m_o(h\omega)}\sum_{n,q}\left|M_{n,q}\right|^2\frac{\Gamma}{\left(E_{n.q}-E_{l,q}-h\omega\right)^2+(\Gamma/2)^2}\left(N_{l,q}-N_{n,q}\right)$$

where e is the magnitude of the electronic charge, n_r is the refractive index of the material, c is the free-space speed of light, ε_o is the free-space permittivity, m_o is the static electron mass, and $h\nu$ is the energy of a photon. $E_{n,q}$ is the energy eigenvalue of a state with wave vector q in the nth subband of a periodic structure, and $N_{n,q}$ is the volume density of electrons in the state $E_{n,q}$. Γ is the linewidth of the phenomenological linewidth to account for scattering broadening. The momentum matrix element for z-polarized light is given by

$$M_{n,q} = \left\langle \phi_{n,q}(z)\left|\frac{-ih}{m_e^*(z)}\frac{\partial}{\partial z}\right|\phi_{l,q}(z)\right\rangle$$

where $f_{n,q}(z)$ is the wave function of the state $E_{n,q}$ and $m_e^*(z)$ is the electron effective mass. The energy eigen values and wave functions are found by solving the one-dimensional Schrödinger's equation for the above periodic potential profile V(z),

$$-\frac{h^2}{2}\frac{\partial}{\partial z}\left[\frac{1}{m_e^*(z)}\frac{\partial}{\partial z}\phi_{n,q}(z)\right]+V(z)\phi_{n,q}(z) = E_{n,q}\phi_{n,q}(z)$$

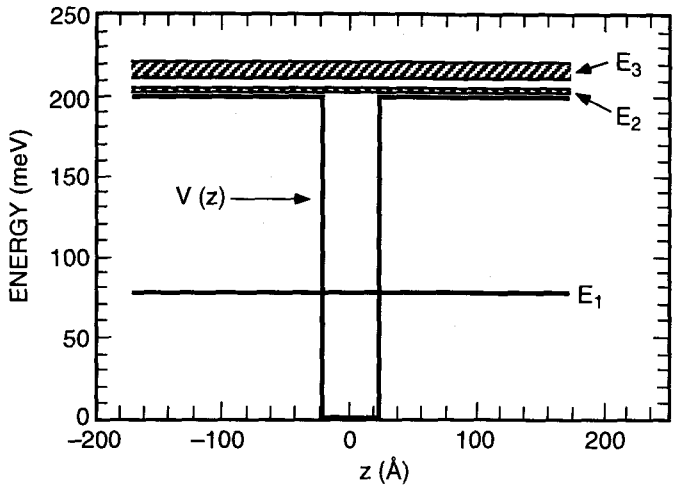

Fig. 2. One period of the MQW structure with its associated energy eigen values for the first four subbands for the as-grown QWIP.

For as-grown AlGaAs/GaAs QWIP to operate in the window of 8-12 μm and have peak response at about 10 μm, the above calculation shows that a quantum well width of 40Å and a barrier width of 300Å can be used, as shown in Fig. 3(a). The actual devices were fabricated exactly to the above design parameters. As we can see from Fig. 3(b), for both QWIP on GaAs or Si substrate the absorption coefficient spectra are in excellent agreement with the theoretical calculation concerning the peak absorption wavelength and general shape.

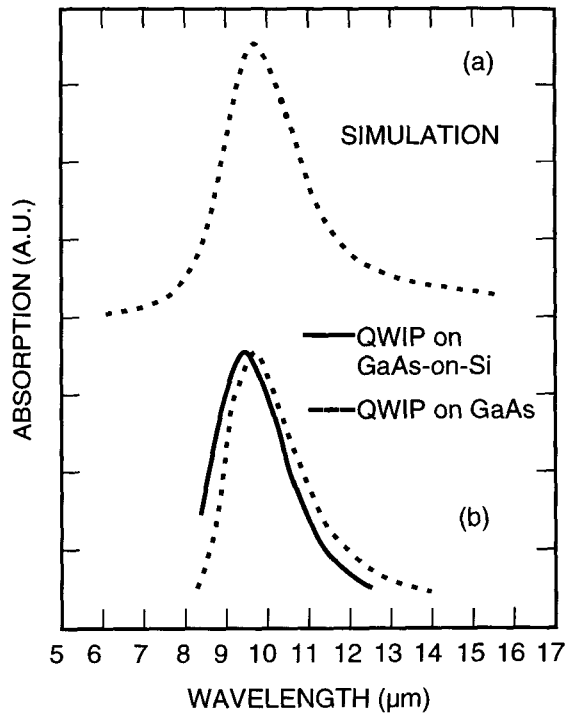

Fig. 3. Calculated and measured absorption characteristics (a) Calculated bound-to-continuum absorption and (b) measured absorption for QWIP on GaAs-on-Si (solid line) and QWIP-on-GaAs (dashed line).

4. RESULTS AND DISCUSSION

(A) MATERIAL PROPERTIES

To characterize the QW detector structure on GaAs-on-Si substrate, both TEM and X-ray diffraction techniques were used. Since there is a 4% lattice mismatch between the Si substrate and the GaAs epitaxial layer, misfit dislocations form along the interface. Due to the islanded growth of GaAs [6] crystalline defects such as threading dislocations and stacking faults are formed. These defects propagate into the epilayer with subsequent growth and can sometimes annihilate each other or get bent away from the active region of the device resulting in lower defect densities in the upper region of the epilayer as shown in Fig. 4. The dislocation density is significantly lower in the as-grown QWIP's active region than at the interface

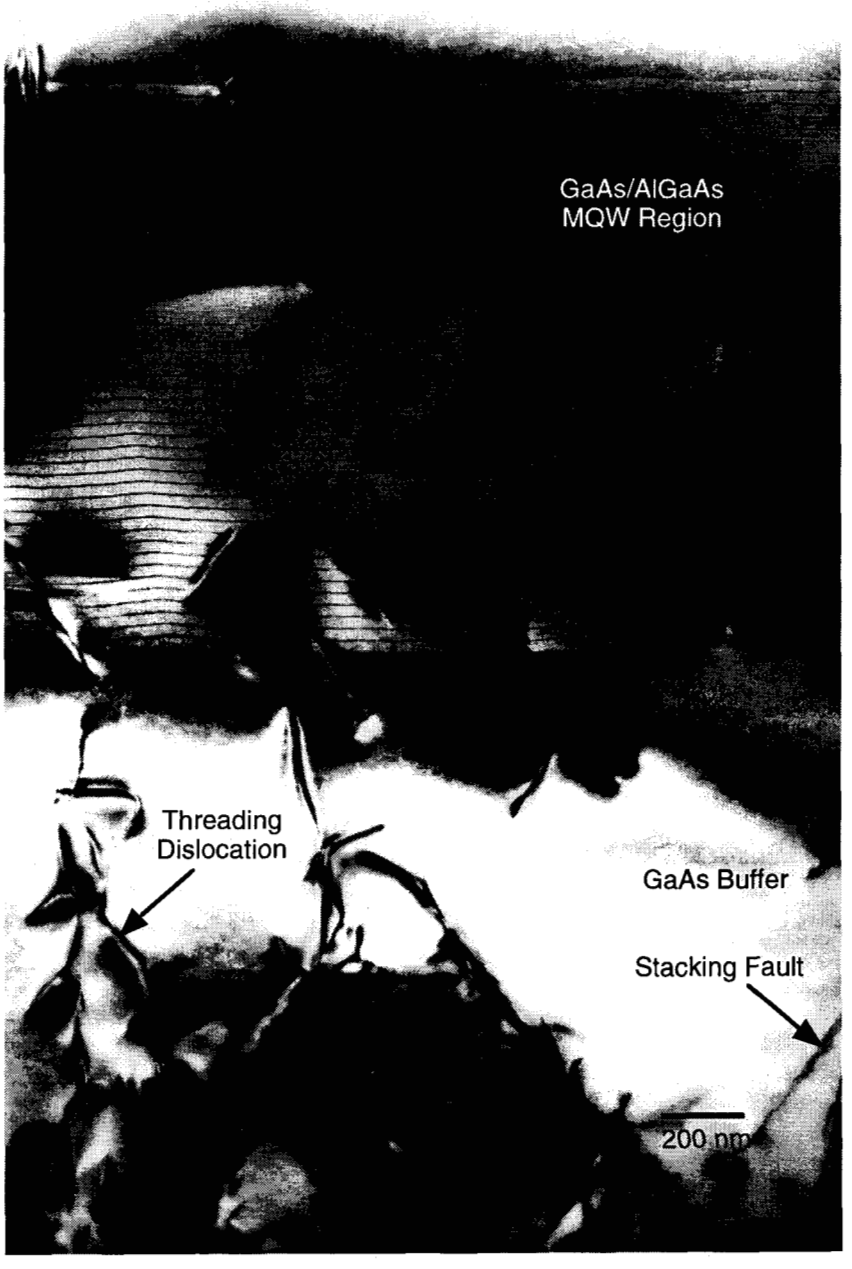

Fig. 4. *Cross-sectional bright field TEM of an as-grown QWIP on GaAs-on-Si substrate. A lesser quantity of defects is observed in the MQW region.*

as indicated in the micrograph in Fig. 7. Figure 5 shows the high resolution lattice imaging of the GaAs/AlGaAs interface with the measured well thickness ~45.2 A°. Also shown in Fig. 6 is the bright-field cross-sectional/TEM image illustrating the interaction between GaAs/AlGaAs superlattices and threading dislocations. Upward propagation of threading dislocation through the growing QW/barrier layers affects the morphology as evidenced in Fig. 6. A single threading dislocation is seen causing the wells to bend around it during growth, perhaps due to a dislocation enhanced growth mechanism. Double crystal X-ray diffraction (DCXRD) was used to determine the crystalline quality of the MOCVD grown GaAs-on-Si buffer layer. The as-grown layer had an FWHM of 342 arc seconds. By annealing the buffer layer an improvement in crystalline quality was observed with the x-ray FWHM dropping to 115 arc seconds as shown in Fig. 7.

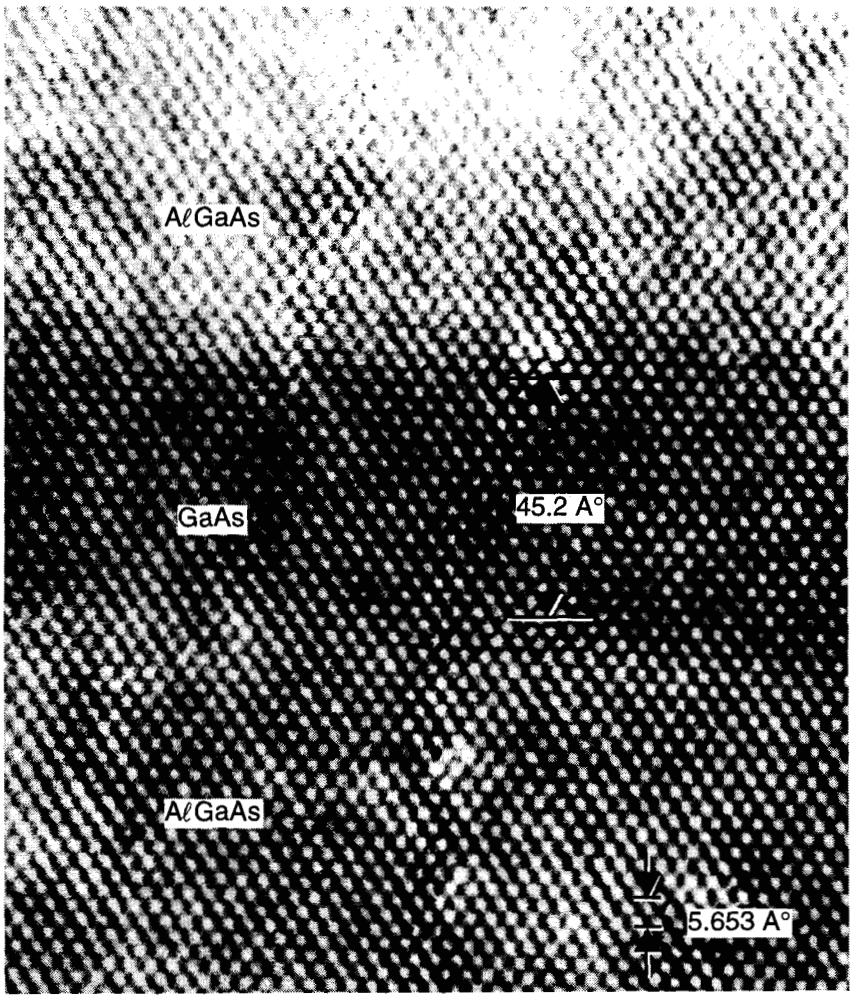

Fig. 5. *High resolution lattice imaging of the GaAs/AlGaAs interface. Measured well thickness ~45.2 A°.*

From the 77K PL spectrum of Fig. 8, a blue shift of 45-angstroms is observed for the detector structure on GaAs-on-Si substrate in comparison to the detector structure grown on GaAs substrate. As grown films of GaAs-on-Si, both by MOCVD and MBE exhibit a red shift in their PL because of the presence of tensile strain in the film. The tensile stress arises due to the difference in thermal expansion coefficients between the GaAs and Silicon. GaAs has a higher thermal expansion coefficient than Silicon and thus contracts faster than Silicon upon cooling from the growth to room temperature. To first order quantum well emission should be immune to the lattice strain since lattice strain at most can cause changes in the band offset which should not affect the ground states significantly. Therefore the explanation obviously lies elsewhere. Due to the island type initial growth for GaAs-on-Si, the surface morphology of the epilayer is not atomically flat and has undulations. These undulations give rise to variations in barrier and well thickness mainly due to the growth anomaly. The 77K PL peak for the QWIP on GaAs peaks at ~7740 angstroms in comparison to 7695 angstroms for the QWIP on GaAs-on-Si indicating a small blue shift for the detector structure grown on a GaAs-on-Si substrate.

Fig. 6. *Bright-field cross-sectional TEM image illustrating the interaction between GaAs/AlGaAs superlattices and threading dislocations.*

The room temperature absorption spectra, shown in Fig. 9, were measured on a 45° polished multipass sample. The absorption of the buffer layer and substrate, either GaAs or Silicon substrate was measured and subtracted from the first spectrum in order to isolate the absorption of the quantum well structure. The peak absorption and the cut-off wavelengths, defined as the long wavelength 50% response, occurred at 9.49 μm and 10.19 μm respectively for the detector structure grown on the GaAs substrate whereas similar detector structure grown on the GaAs-on-Si substrate peaks at 9.6 μm with a broad shoulder arising mainly from the growth anomaly. The broad intersubband absorption is due to the transitions from bound states in the wells to the continuum band above the energy barriers.

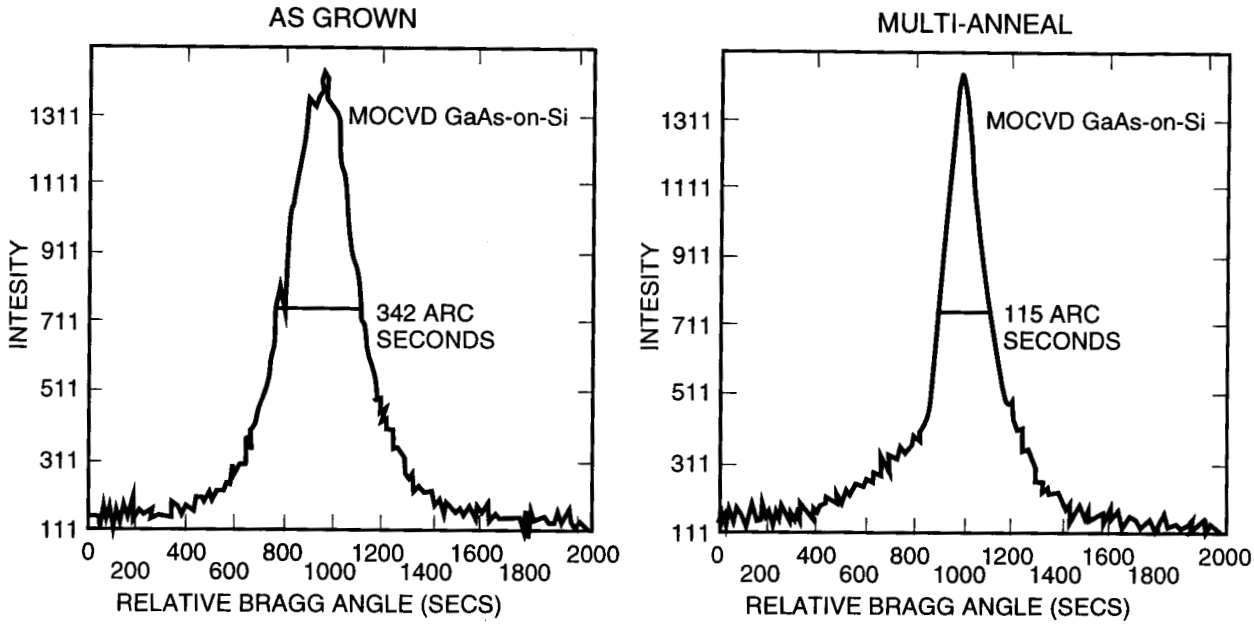

Fig. 7. *Double crystal x-ray diffraction rocking curve of GaAs-on-Si substrate.*

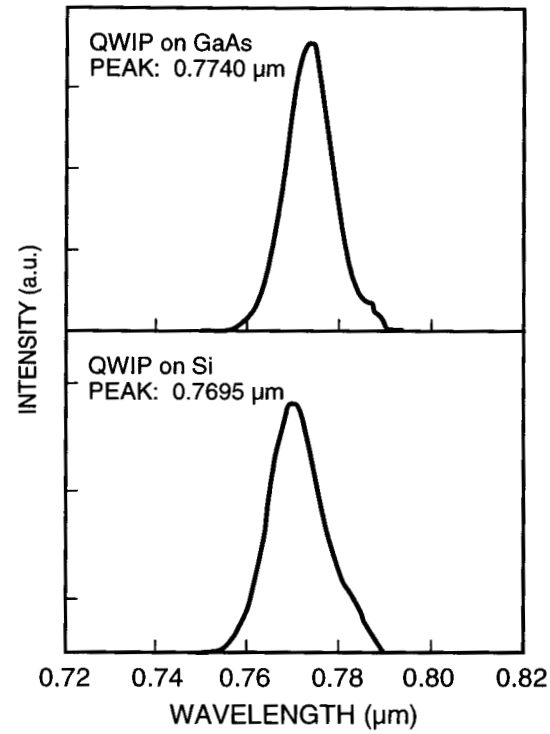

Fig. 8. *Comparison of the photoluminescence responses for the QWIP on GaAs-on-Si and QWIP on GaAs structure.*

(B) DEVICE CHARACTERISTICS

The dark current measured as a function of voltage and temperature is shown in Figs. 10(a) & (b) for the quantum well detector structures grown on GaAs and on GaAs-on-Si substrates, respectively. The detector structure grown on a GaAs-on-Si substrate exhibits higher dark current in comparison to the detector structure grown on a GaAs substrate as shown in

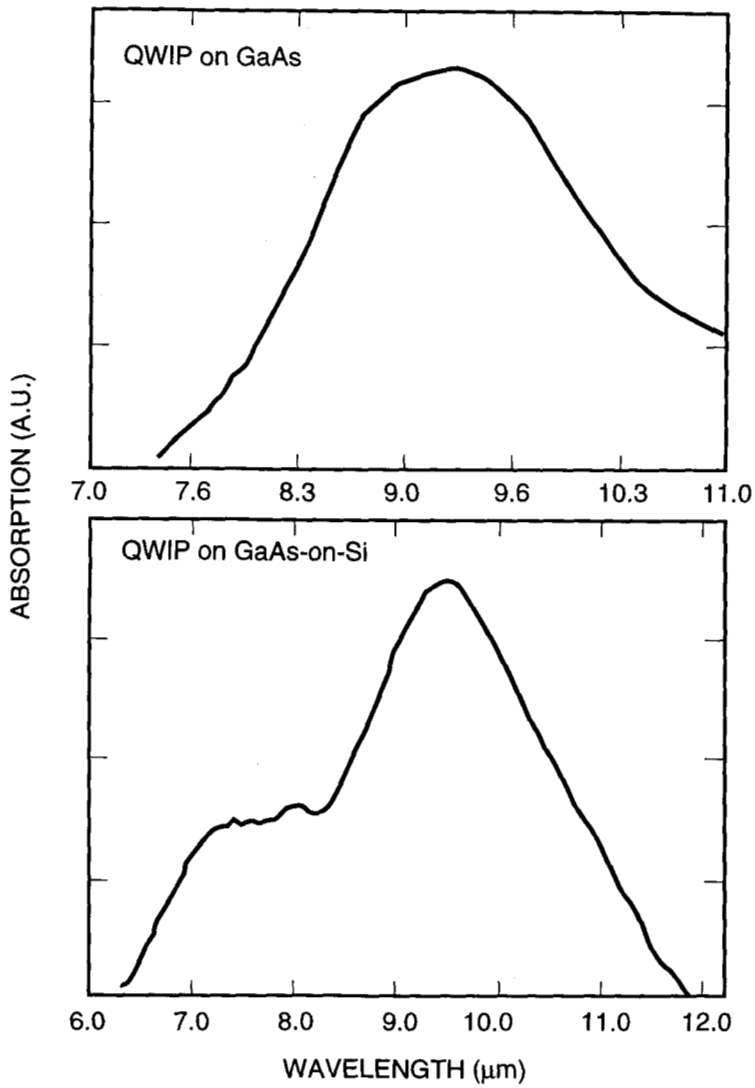

Fig. 9. *Room temp intersubband absorption of QWIP on GaAs and QWIP on GaAs-on-Si structures.*

Fig. 11. At low temperatures, the difference in dark current is speculated to be due to defect assisted tunneling. Both the detectors exhibit a decrease in the dark current with decreasing temperature. Fig. 12 shows the comparison of bias dependence of activation energy of QWIP on GaAs-on-Si versus QWIP on GaAs substrates. Nearly identical activation energy versus bias characteristics is observed for both detectors. The decrease in the activation energy with bias is attributed to the decrease in the effective barrier height with bias.

Fig. 13 shows the 77°K relative spectral response of the QWIP on GaAs and the QWIP on GaAs-on-Si detectors measured at 4.0 V bias. The response curves have been scaled so that the peak position and line shape may be compared. The QWIP on GaAs-on-Si detector has a peak response at 8.41 μm, while the peak response of the QWIP on GaAs is at 8.62 μm. The small blue shift (0.21 μm) in the peak response of the QWIP on GaAs-on-Si detector is possibly due to the presence of some residual strain in the lattice.

The 77°K absolute responsivity as a function of bias is shown in Fig. 14. At bias voltages of +2.5 and -2.5 V, peak absolute responsivity of 0.53 and 0.47 A/W were measured for the QWIP on GaAs detector, while 0.47 and 0.40 A/W were measured for the QWIP on GaAs-on-Si detector. Similar to the asymmetry in dark current versus voltage, the asymmetry in responsivity versus voltage seen in Fig. 12 may be attributed to growth related effects.

The unity gain quantum efficiency was calculated from the absolute response. The peak quantum efficiency were 7.62% for the QWIP on GaAs detector as compared to 6.92% for the QWIP on GaAs-on-Si detector. The resulting QWIP on the GaAs-on-Si detector exhibits quantum efficiency comparable to a similar detector structure grown on a GaAs substrate thus making it a contender for IR imaging systems.

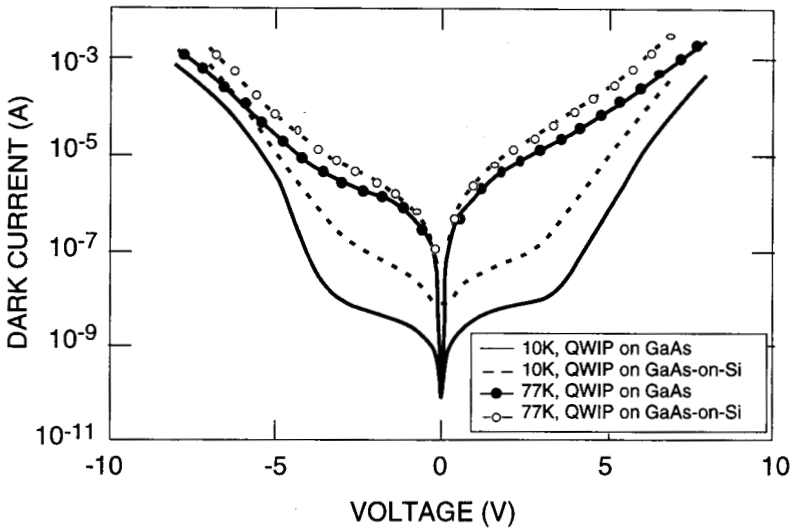

Fig. 11. Comparison of the dark current versus bias for QWIP-on-GaAs and QWIP-on-GaAs-on-Si detectors.

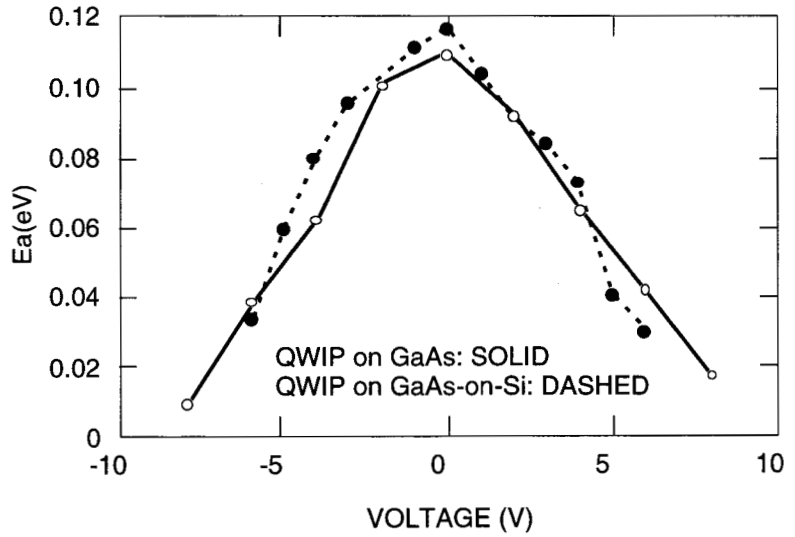

Fig. 12. Comparison of the activation energy versus bias for QWIP-on-GaAs and QWIP-on-GaAs-on-Si detectors.

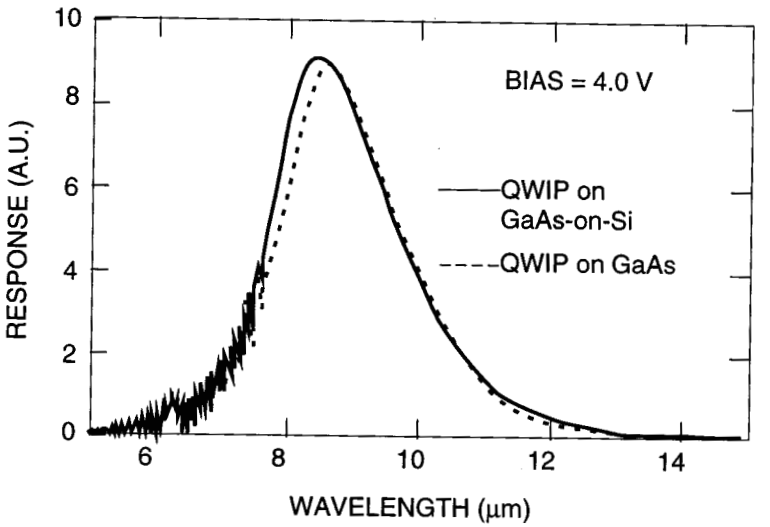

Fig. 13. Comparison of the relative spectral responses for the QWIP-on-GaAs-on-Si and QWIP-on-GaAs detectors. Response curves have been scaled to yield similar peak values.

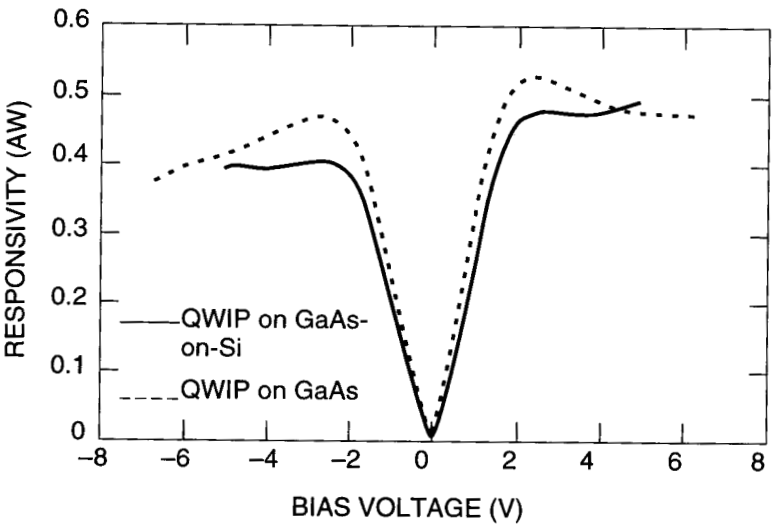

Fig. 14. Comparison of the absolute responses for the QWIP-on-GaAs and QWIP-on-GaAs-on-Si detectors.

5. CONCLUSION

In conclusion, we have performed room-temperature infrared absorption, dark current-bias voltage measurements as a function of temperature and photo response measurements for GaAs multi-QW IR detector grown on GaAs-on-Si substrates. These results were compared to measurements performed on the same structure grown on GaAs substrate. We find that the detector structure grown on a Silicon substrate partially relaxes as revealed by the presence of dislocations in the MWQ lattice and exhibits a small blue shift in the response. The dark current measurements suggest that further research is needed to achieve higher performance long wavelength photodetectors. These initial results show promise for the growth of QWIP detectors on silicon wafers and applications for integration with silicon-based electronics. The results are promising for applications in the important 8-12 μm atmospheric window.

6. ACKNOWLEDGMENTS

Research described in the paper was performed by the Center for Space Microelectronics Technology, Jet Propulsion Laboratory, California Institute of Technology, Pasadena, CA 91109 and was sponsored by the NASA office of Space Science Access and Technology, and by the Microelectronics Laboratory, University of Illinois at Urbana-Campaign, Urbana, IL 61801. The authors would like to acknowledge Profs. N. Holonyak Jr., M. Feng, S.L. Chuang, and K.C. Hseih of University of Illinois at Urbana-Champaign and Dr. K.K. Choi of US Army Research Lab, New Jersey for many helpful discussions. We would also like to acknowledge D. Cuda (JPL) for help with the manuscript preparation. One of the authors (D.K.S.) acknowledges the fellowship awarded by the National Academy of Sciences – National Resarch Council.

7. REFERENCES

1. B.F. Levine, "Quantum-well Infrared Photodetectors", J. Appl. Phys. 74, R1 (1993).

2. S.D. Gunapala, S.V. Bandara, J.K. Liu, W. Hong, E.M. Luong, J.M. Mumolo, M.J. McKelvey, D.K. Sengupta, A. Singh, C.A. Schott, R. Carralejo, P.D. Maker, J.J. Bock, M.E. Ressler, M.W. Werner, and T. Krabach, "Quantum Well Infrared Photodetector Research and Development at Jet Propulsion Laboratory," Proc. SPIE, Vol. 3379, to be published.

3. M. Akiyama, Y. Kawarada, S. Nishi, T. Ueda, and K. Kaminishi, "Growth of GaAs on Si and Its Application to FETs and LEDs," Mater, Res. Soc. Symp. Proc. 67, 53 (1986).

4. H. Schichijo, L. Tran, R. Matyi, and J. Lee, "Prospects for GaAs-on-Si LSI Circuits," Mater. Res. Soc. Symp. Proc. 91, 201 (1987).

5. C. Ifo, M. Feng, V.K. Eu, and H.B. Kim, "High Volume Production Growth of GaAs on Silicon Substrates," Mater. Res. Soc. Symp. Proc. 67, 197 (1986).

6. T. George, "Defect Generation Mechanisms in MOCVD-Grown Gallium Arsenide Heteroepitaxial Layers on Silicon Substrates," Ph.D Thesis, Materials Science and Mineral Engineering, University of California at Berkeley.